Colloids and Surfaces A: Physicochem. Eng. Aspects 511 (2016) 329–338

Contents lists available at ScienceDirect

Colloids and Surfaces A: Physicochemical and Engineering Aspects

journal homepage: www.elsevier.com/locate/colsurfa

Fabrication, characterization, and visible-light photocatalytic performance of ternary plasmonic composites

Fei Chang[a,*], Junrong Sun[a], Jie Wang[a], Xiaofang Wang[a], Baoqing Deng[a], Xuefeng Hu[b,*]

[a] School of Environment and Architecture, University of Shanghai for Science and Technology, Shanghai, 200093, PR China
[b] Key Laboratory of Coastal Environmental Processes and Ecological Remediation, Yantai Institute of Coastal Zone Research, Chinese Academy of Sciences, Yantai, Shandong, 264003, PR China

HIGHLIGHTS

- W-Ti-SBA15 composites with low TiO_2/SiO_2 mass ratios and their Ag-contained analogs were fabricated.
- These composites showed enhanced photocatalytic performance in comparison to those with high TiO_2/SiO_2 mass ratios.
- Photocatalysis mechanism of these Ag-W-Ti-SBA15 plasmonic composites was proposed.

GRAPHICAL ABSTRACT

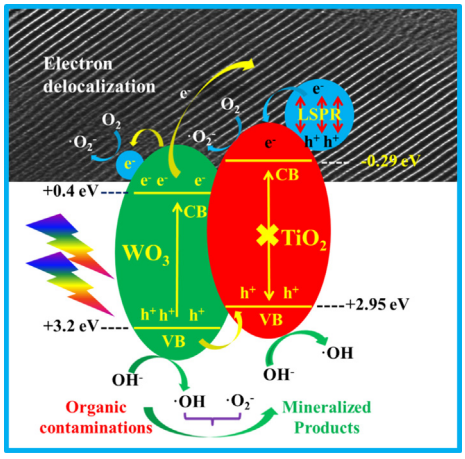

ARTICLE INFO

Article history:
Received 2 August 2016
Received in revised form
29 September 2016
Accepted 11 October 2016
Available online 12 October 2016

Keywords:
Ag-W-Ti-SBA15
Visible-light driven
Plasmonic
Photocatalytic
Mechanism

ABSTRACT

A group of mesoporous WO_3-TiO_2-contained SBA15 composites (W-Ti-SBA15) and their Ag-contained plasmonic analogs were fabricated and then systematically characterized by a collection of analytical techniques. Original mesoporous structures with highly ordered channels were well-maintained and WO_3-TiO_2 could form spherical clusters that were gradually reduced in size accompanying with the decrease of TiO_2/SiO_2 mass ratios. Deposited Ag species were confirmed as zero-valence Ag by X-ray photoelectron spectroscopy analysis and exerted almost no effect on the morphology, microstructure, and textural but optical property, by which the visible-light harvesting ability of composites was remarkably strengthened owing to the localized surface plasmonic resonance (LSPR) induced by the metallic Ag. Under visible-light irradiation, W-Ti-SBA15 composites showed satisfactory photocatalytic performance that could be further enhanced by using their Ag-contained ternary plasmonic analogs. The enhancement of photocatalytic efficiency was mainly attributed to the favorable mesoporous morphology, the suitable band alignment, and the LSPR effect. Eventually, a possible photocatalysis mechanism was primarily proposed on the base of reactive radical species trapping experiments.

1. Introduction

It is well recognized that anatase (TiO_2) is an excellent heterogeneous photocatalyst to mediate environmental contaminants

* Corresponding authors.
E-mail addresses: feichang@usst.edu.cn (F. Chang), xfhu@yic.ac.cn (X. Hu).

http://dx.doi.org/10.1016/j.colsurfa.2016.10.024
0927-7757/

removal, evolution of gaseous hydrogen, and selective organic conversion in ultraviolet region, owning to the favorable physicochemical properties [1–3]. For practical applications, the TiO_2 should be modified in terms of microstructure and morphology to pursue the extension of light absorption range, the enhancement of photocatalytic performance, and the ease of recovery after utilization [4]. Among several modification strategies that currently intensively researched, the construction of a composite containing TiO_2 and another semiconductor component with an appropriate band structure is an effective manner to strengthen the visible-light harvesting and photocatalytic capability as a result of the inhibited recombination of photoinduced charge carriers [5].

Tungsten oxide (WO_3) with a relatively narrow band gap (~2.4 eV) has been extensively applied in various fields such as electrochromic devices, dye-sensitized solar cells, gas sensors, and photocatalytic processes [6,7]. It is usually adopted as a suitable candidate to fabricate composites together with TiO_2, attributing to the well-matched band gap structure [8–12]. The generated charge carries are able to migrate across heterojunction interfaces towards different components and the recombination of charge carries is thus effectively retarded, hereby improving photocatalytic efficiency [13–15]. In addition, the integration of WO_3 into composites induces the enhancement of surface acidity, by which some species with unpaired electrons like O_2, H_2O, and OH^- are prone to access active sites and convert to oxidative O_2^- and $^{\bullet}OH$ radicals, thus boosting photocatalytic performance [16–18]. If the produced composite incorporates into an appropriate matrix like SBA15, much more active sites can be exposed originating from the decreased particle size and a large amount of pollutant molecules tend to gather around active sites as a result of the strengthened adsorption ability from support, further benefiting photocatalytic processes [19–22].

The deposition of noble metal nanoparticles on surface of semiconductors is another efficient manner to promote photocatalytic efficiency through the formation of schottky junction at the metal-semiconductor interfaces and the LSPR effect by metallic noble elements [23–25]. The former is able to induce the directional migration of electrons and hereby causes the separation of charge carriers [26,27]. The later can enhance the visible-light adsorption and boost the generation of charge carriers. Among mostly used noble metals such as Ag, Pt, Pb, Au, Ag is quite promising due to the low toxicity, antibacterial activity, easy preparation and controllable morphology [28].

In a previous study, the synthesis and photocatalytic assessment of mesoporous W-Ti-SBA15 composites were investigated, and these heterojunction-structured composites showed enhanced photocatalytic efficiency in comparison to single-component samples [29]. However, the photocatalytic performance was not as that good as we had expected, mainly attributing to the serious aggregation of TiO_2 particles since the excess amount of titanium precursor was added during synthesis. In order to achieve the further advancement of photocatalytic performance, in this study we tried to reduce the mass ratio of TiO_2/SiO_2 for the sake of the maximal exposure of active sites to contaminant molecules. In addition, silver nanoparticles were introduced on the surface of above composites to construct a ternary Ag-W-Ti-SBA15 plasmonic system. As far as we know, there is no relevant investigation regarding the construction and photocatalytic evaluation of ternary Ag-W-Ti-SBA15 plasmonic composites.

In the current study, a series of W-Ti-SBA15 composites and their Ag-decorated counterparts were fabricated and were fully characterized. The original mesoporous structure was well conserved even after decorating metallic Ag species. W-Ti-SBA15 composites showed satisfactory photocatalytic performance toward the degradation of dye rhodamine B (RhB) under visible-light irradiation. As expected, Ag-contained Ag-W-Ti-SBA15 plasmonic composites exhibited relatively high photocatalytic efficiency comparing with their W-Ti-SBA15 analogs. The enhancement of catalytic outcome was discussed and a possible photocatalysis mechanism was proposed basing upon active species trapping experiments.

2. Materials and methods

2.1. Materials

Pluronic P123 ($PEO_{20}PPO_{70}PEO_{20}$) and sodium tungstate ($Na_2WO_4{\cdot}2H_2O$) were purchased from Aldrich Chemical Co. and ACROS Organics, respectively. Hydrochloric acid (HCl, 36–38%, AR), silver nitrate ($AgNO_3$, AR), titanium sulfate ($Ti(SO_4)_2{\cdot}9H_2O$, CP), tetraethyl orthosilicate (TEOS, $Si(OC_2H_5)_4$, AR), nitroblue tetrazolium (NBT, AR), and other chemicals involved were obtained from Sinopharm Chemical Reagent Co., Ltd. (Shanghai, China) and used directly as received without further purification. Rhodamine B (RhB, AR) was purchased from Shanghai SSS Reagent Co., Ltd. (Shanghai, China). Deionized water was used throughout the experiment.

2.2. Synthesis of W-Ti-SBA15 composites

The synthetic procedure was similar to the previous study except that the amount of titanium and tungsten precursors was greatly reduced [29]. A series of W-Ti-SBA15 mesoporous composites were prepared and nominated as 5%WTSx, where 5% and x were defined as theoretical mass ratios of formed WO_3/TiO_2 and TiO_2/SiO_2, respectively. Sample WO_3/TiO_2 with a mass ratio of 5% was fabricated according to a same procedure as above except the absence of silicon source and denoted as 5%WT. In addition, N-doped TiO_2 (N-TiO_2) was synthesized in the light of a previous report for comparison [30].

2.3. Synthesis of Ag-W-Ti-SBA15 plasmonic composites

Since the as-synthesized sample 5%WTS0.1 showed the best photocatalytic behavior and was specifically selected to prepare Ag-W-Ti-SBA15 plasmonic composites. In a typical procedure, the sample 5%WTS0.1 (1 g) in deionized water (40 mL) was ultrasonicated for 30 min to make a suspension that was subsequently added with a desired amount of $AgNO_3$. After a vigorous stir of 900 r/min (JB-2A constant temperature agitator, Shanghai INESA Scientific Instrument Co., Ltd, China) at room temperature for 5 h in dark, methanol (20 mL) was added into the reaction system that was then exposed to a 400 W halogen lamp (Institute for Electric Light Source, Beijing) equipped with a $NaNO_2$ solution (2 M) to remove ultraviolet-light (<400 nm) for 20 min. The resultant precipitate was collected by centrifugation, washed with ethanol and deionized water for at least five times to completely remove silver cations, and dried at 60 °C for 12 h to provide final products. For simplicity, these composites were denoted as xAgWTS and x herein was referred to a theoretical mass ratio of Ag versus WTS.

2.4. Characterizations

Powder X-ray diffraction (XRD) patterns were recorded on a Bruker D8 Advance X-ray diffractometer (Bruker AXS, Germany) using a Cu Kα radiation source (λ = 1.5406 Å). The X-ray photoelectron spectroscopy (XPS) measurements were conducted on a Thermo Scientific ESCALAB 250XI system. Binding energies were calibrated with the containment carbon (C1s = 284.6 eV). The morphology and microstructure of obtained samples were recorded on transmission electron microscopy (TEM, JEOL JEM-2011) and the chemical composition of samples was determined by X-ray energy dispersion spectroscopy (EDS). The specific surface areas were mea-

sured by nitrogen adsorption-desorption isotherms at 77 K using a Micromeritics 3Flex apparatus. Before measurement, the samples were degassed at 423 K under vacuum over 6 h. UV–vis diffuse reflectance spectra (UV–vis DRS) were performed on a Shimadzu UV-2600 spectrophotometer using $BaSO_4$ as a reference.

2.5. Photocatalytic activity assessment

Photocatalytic evaluation experiments were conducted through the degradation of dye RhB under visible-light irradiation using a 300 W xenon lamp (CEL-HXF300, AuLight, Beijing) with a 420–780 nm cut-off filter. The photocatalyst (40 mg) was dispersed into to an RhB aqueous solution (15 mg L^{-1}, 80 mL). Prior to the light irradiation, the suspension was vigorously stirred (900 r/min, JB-2A constant temperature agitator, Shanghai INESA Scientific Instrument Co., Ltd, China) for 1 h to reach an adsorption saturation of organic molecules onto the surface of catalyst particles. After degradation reactions occurred, 4 mL aliquot was sampled, diluted, and centrifuged at 10000 rpm for 5 min (TGL–20 B centrifugal machine, Shanghai Anting Scientific Instrument Factory, China) to remove catalyst particles at every 30 min. The residue concentration of RhB was evaluated through a UV–vis spectrophotometer (Purkinje General T6) at 554 nm.

Several active radical species possibly generated during photocatalytic reactions were detected in order to propose a mechanism. Specifically, 1.0 mM isopropanol alcohol (IPA) or disodium ethylenediaminetetraacetate (EDTA-2Na) was introduced to check the presence of hydroxyl radicals (•OH) or produced holes (h^+) [31,32]. In addition, 25 μM nitroblue tetrazolium (NBT) was added into reaction system in place of RhB to analyze superoxide radicals ($•O_2^-$) that might probably produce [33].

Each reported value as above was the average of at least three parallel tests and the corresponding standard deviation was calculated within ±3%.

3. Results and discussion

Low-angle and wide-angle XRD patterns of obtained 5%WTSx composites with variable TiO_2/SiO_2 mass ratios are represented in Fig. 1A and B, respectively. All samples in Fig. 1A exhibit three well-resolved peaks in low-angle X-ray diagrams, assigning to characteristic reflections of (100), (110), and (200) crystal planes that originate from mesoporous silicon-based materials with *p6mm* hexagonal symmetry [34]. It is obvious that the involvement of external species has almost no effect on the SBA15 original structure. In Fig. 1B, a series of peaks at approximately 25.6°, 38.2°, 48.4°, 54.4°, 55.4°, 63.1° assigned to the extra-framework tetragonal anatase TiO_2 phase (JCPDS No.21-1272) [10,16] are clearly observed in all samples, even the one with quite low TiO_2/SiO_2 mass ratio of 0.025, possibly attributing to the much higher condensation rate and thus the easier generation of titania clusters in aqueous environment than silica [35]. The intensity of peaks is gradually reduced with the abatement of TiO_2/SiO_2 mass ratios, suggesting the stepwise decrease of the amount and crystallinity of anatase. A broad band at around 23° is attributed to amorphous or microcrystalline phase of silica [36]. However, there are no diffraction reflections corresponding to WO_3 phase and solid solution of $W_xTi_{1-x}O_2$ [37], revealing the uniform distribution of WO_3 onto TiO_2 matrix and the inexistence of other impurities [9]. The integration of metallic Ag species into WTS samples exerts almost no effect on the original mesoporous structures since three feature diffraction signals are prominent in Fig. 1C. In addition, quite similar diffraction patterns of Ag-contained ternary composites to those WTS series are observed in Fig. 1D and the absence of metallic Ag signals is mainly due to the uniform dispersion or the overlap of (111) crystal plane in metallic Ag phase at 38.1° by the (004) crystal plane in anatase TiO_2 at 38.2° [38].

Table 1
S_{BET}, pore volume, and band gap energies of 5%WTSx series and xAgWTS series.

Composites	S_{BET} ($m^2\ g^{-1}$)	Pore volume ($cm^3\ g^{-1}$)	Band gap (eV)
5%WTS0.2	590.9	0.666	2.95
5%WTS0.1	719.7	0.694	2.97
5%WTS0.05	899.4	0.852	2.98
5%WTS0.025	838.1	0.711	3.12
5%AgWTS	743.3	0.726	3.24
10%AgWTS	712.5	0.714	3.26
15%AgWTS	699.4	0.663	3.26
20%AgWTS	682.7	0.739	3.28

The morphology and microstructures of as-prepared composites were observed by TEM images and are depicted in Fig. 2. All WTS samples with low TiO_2/SiO_2 mass ratios possess extremely ordered and uniform mesoporous microstructures. As seen in Fig. 2A–D, both the quantity and size of the black spherical clusters anatase TiO_2 are gradually decreased along with the decrease of Ti species concentration, which is in good accordance with the XRD analyses. The EDS spectrum of the sample 5%WTS0.1 in Fig. A1 shows four elemental sepecies W, Ti, Si, and O and mass ratios of WO_3/TiO_2 and TiO_2/SiO_2 are estimated as 0.042 and 0.094 that are quite close to theoretical values. After the decoration of metallic Ag, the original mesoporous structure with regular parallel channels is well maintained in sample 5%AgWTS, as shown in Fig. 2E. Two distinct lattice fringes of 0.350 nm and 0.242 nm are observed in HRTEM image and correspond to crystallographic planes of (101) and (111) in anatase TiO_2 phase and metallic Ag in Fig. 2F. However, no obvious lattice fringes assigning to WO_3 are found in such circumstance.

The N_2 adsorption-desorption isotherms were checked to investigate the textural property of as-synthesized composites, as represented in Fig. 3. It is observed that all composites display the identical type IV isotherms with a typical H1 hysteresis loop in a relative pressure P/P_0 range from 0.5 to 0.9, suggestive of regular mesoporous mcirostructures with hexagonal cylindrical pores at capillary condensation step [39], which is in good agreement with the analytic results from XRD patters and TEM images. Specific surface area (S_{BET}) and pore volume values of these mesoporous composites are collected in Table 1. As expected for WTS series, with the reduction of TiO_2/SiO_2 mass ratio, specific surface area and pore volume values are gradually increased, revealing that Ti and W alien species mainly exist as large clusters on the external surface of SBA-15 support and the higher TiO_2/SiO_2 mass ratio induces the less ordered mesoporous materials with the lower specific surface area [40]. As to composites AgWTS with the increase of Ag precursor addition, specific surface area values are slightly decreased while the average pore diameters keeps almost in variant, indicating that the presence of small amount of Ag exerts an inconspicuous effect on the textural property.

The optical property of obtained composites was analyzed by UV–vis diffuse reflectance spectra and shown in Fig. 4. It is evident that the photoresponse of WTS series is merely in UV-light region and the adsorption edge is close to 400 nm, corresponding to the O^{-2}–Ti^{+4} charge transition of extra-framework anatase TiO_2. The intensity of the band at about 330 nm increases along with the raise of anatase content, owning to the low structural integrity caused by the comparably high concentration of alien species [41]. A weak band at about 210–230 nm in all samples except 5%WT0.2 is relevant to the isolated tetrahedral Ti^{+4} cations in framework [41], suggesting the relatively high TiO_2/SiO_2 mass ratio tends to promote the formation of extra-framework anatase TiO_2. In addition, with the abatement of TiO_2/SiO_2 mass ratios, the adsorption edge of WTS series is gradually blue-shifted in Fig. 4A, mainly relating to the size shrinkage of anatase TiO_2 clusters in SBA-15 matrix. As soon as metallic Ag was deposited, the photoresponse range of samples is able to extend to the visible-light region, ascribing to the

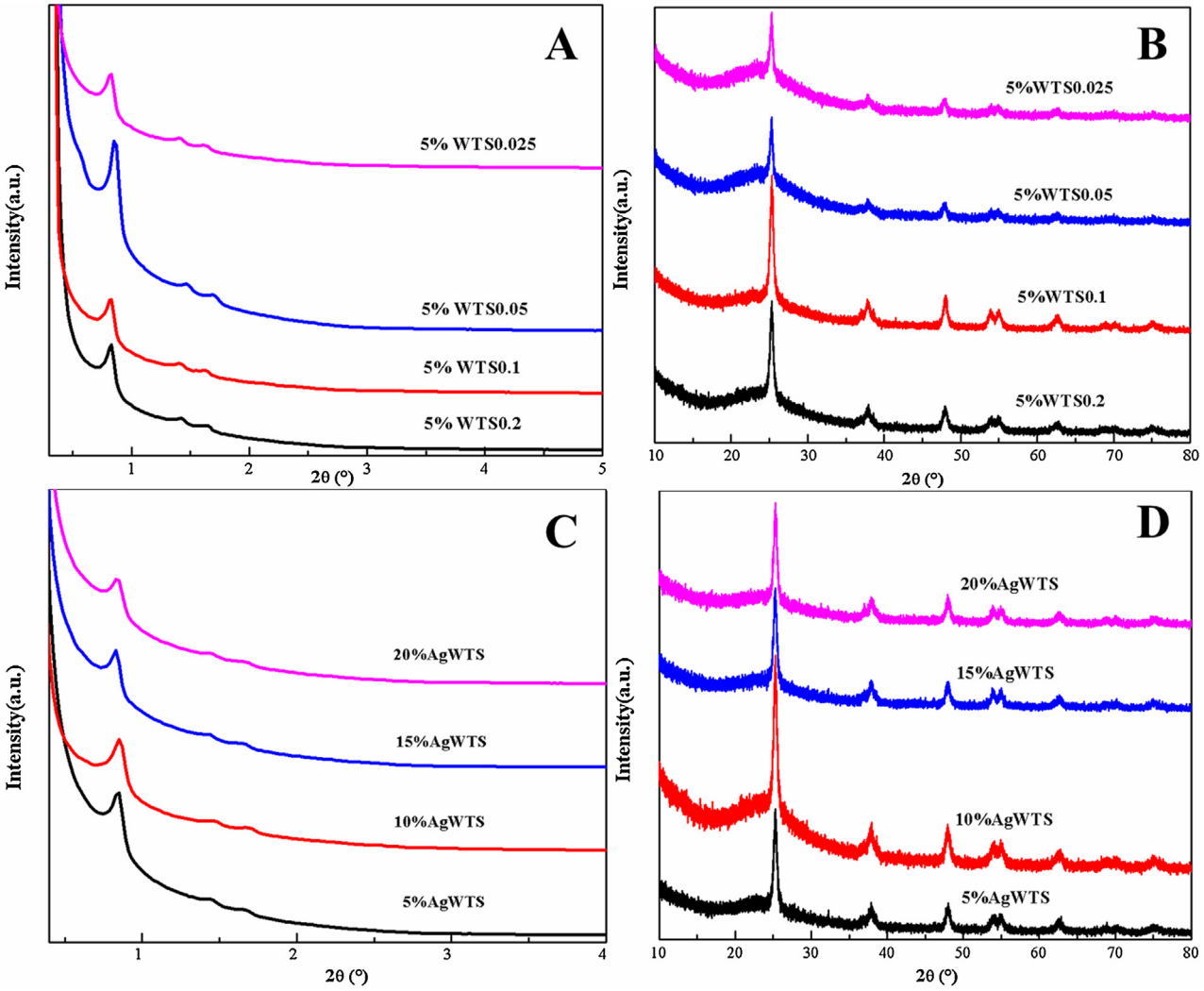

Fig. 1. Low-angle (A) and wide-angle (B) XRD patterns of 5%WTSx series; low-angle (C) and wide-angle (D) XRD patterns of xAgWTS series.

LSPR effect of plasmonic metallic Ag species [42]. Band gap energies (E_g) of these semiconductors were estimated *via* an empirical equation $\alpha h\nu = A(h\nu\text{-}Eg)^{n/2}$ and α, ν, E_g and A refers to the absorption coefficient, light frequency, band gap energy, and a constant, respectively. It is generally realized that anatase TiO_2 undergoes an indirect transition and correspondingly n is set as 4 [31]. As listed in Table 1, E_g values increase with the decrease of TiO_2/SiO_2 mass ratio in WTS series and the increase of Ag deposition in AgWTS series.

To further confirm the presence of Ag species and check the surface valence states, sample 5%AgWTS was selected for XPS analysis with C1s at 284.6 eV as a reference. Clearly, the survey spectrum provides five elements Ti, O, Si, Ag, and W in Fig. 5A, confirming the indeed presence of ternary components as anticipated. There are two peaks with binding energies located at 373.63 eV and 367.63 eV in high resolution spectrum of the Ag 3d spectrum in Fig. 5B, assigning to Ag 3d3/2 and Ag 3d5/2, respectively. The existence of both Ag peaks with the description of 6.0 eV verifies the formation of zero-valence Ag species instead of Ag ions in composites [43]. Fig. 5C displays two prominent signals at around 458.5 eV and 464.2 eV that are indexed to the Ti $2p_{3/2}$-Ti $2p_{1/2}$ spin-orbit components of Ti^{4+} species in anatase TiO_2 lattice [8,15]. W species can be found in Fig. 5D and the band was deconvoluted to two peaks centered at 35.8 eV and 37.9 eV in binding energy owning to the spin-orbit splitting of W (4f) components [44]. In addition, the former peak at 35.8 eV is generally considered as an integration signal composed of the Ti^{4+} species (Ti 3p) in TiO_2 phase and W(4f) ingredients [15].

Photocatalytic performance of obtained composites was estimated by the decomposition of dye RhB under visible-light illumination and repeated at least twice. As depicted in Fig. 6A, the direct photolysis of RhB can be ignored even after 180 min, revealing the sufficient stability of RhB upon such condition. The standard sample N-TiO_2 is able to supply a quite weak photocatalytic removal efficiency of around 23%. Without the mesoporous silicate matrix, the sample 5%WT can catalytically destroy around 39% of RhB molecules that is much lower than those from WTS series with variable TiO_2/SiO_2 mass ratios. Particularly, under the identical condition the best candidate 5% WTS0.1 has an optimal photocatalytic degradation efficiency of 63% that is significantly better than that of 5%WTS0.7, a sample with a large TiO_2/SiO_2 mass ratio of 0.7. The enhancement of photocatalytic behavior of composites with low TiO_2/SiO_2 mass ratios is mainly attributed to the enlarged specific surface areas of composites and good exposure of active sites induced by the decreased size of semiconductor clusters, which facilitates the adsorption of organic molecules near to SBA-15 matrix and further easy access to active sites to undergo degradation reactions. As a result, the sample 5% WTS0.1 was typically selected to construct Ag-contained ternary plasmonic AgWTS composites. Under the same condition, all Ag-contained composites exhibit relatively high photocatalytic performance comparing

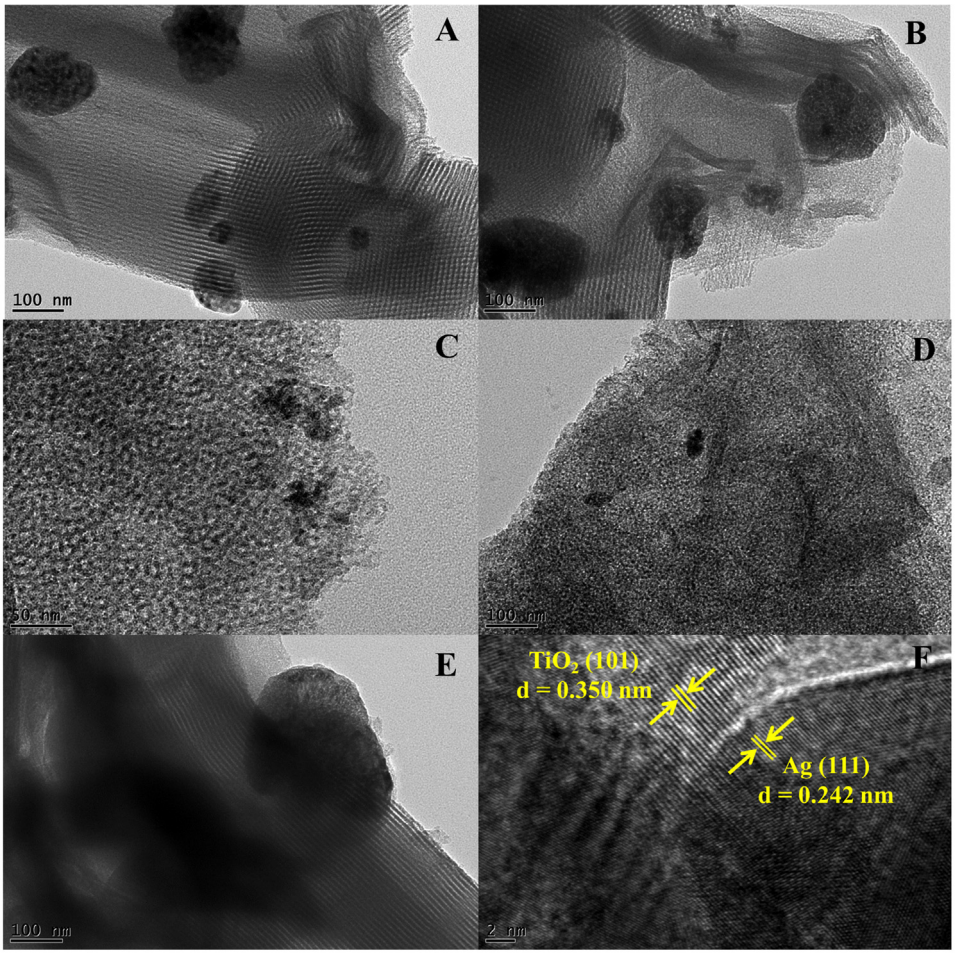

Fig. 2. TEM images of samples: (A) 5%WTS0.2, (B) 5%WTS0.1, (C) 5%WTS0.05, (D) 5%WTS0.025, (E) 5%AgWTS; HRTEM image of sample 5%AgWTS (F).

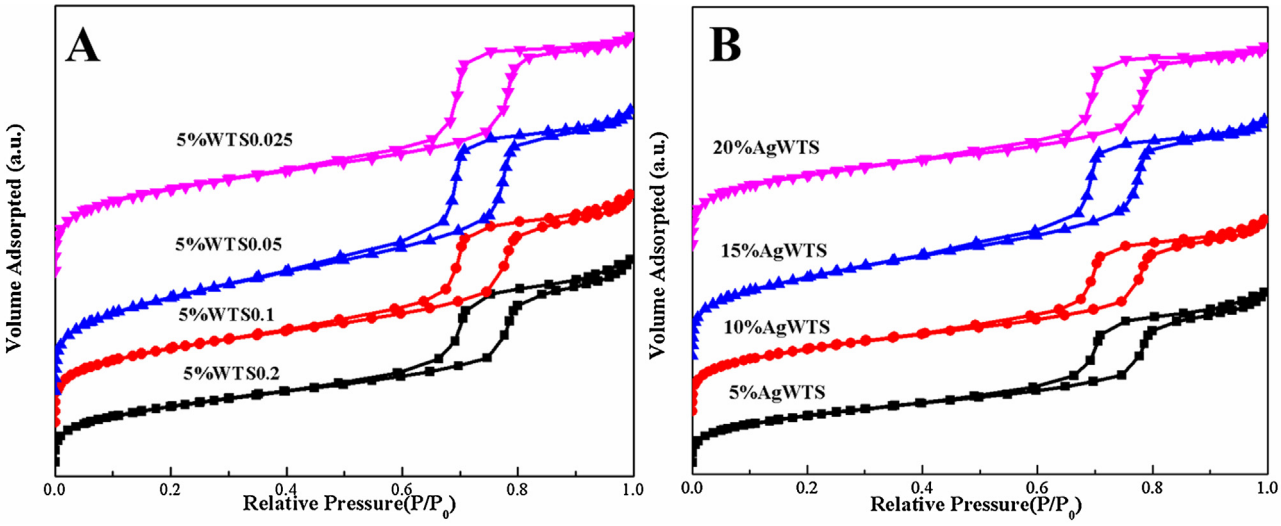

Fig. 3. N_2 adsorption-desorption isotherms of various 5%WTSx samples (A) and xAgWTS samples (B).

to samples without the Ag decoration, as seen in Fig. 6B. The composite with an Ag mass ratio of 5% shows the best photocatalytic outcome among several Ag-deposited systems, indicating that 5% is a suitable mass ratio and excess amount of Ag deposition might role as recombination center of charge carriers, hereby inhibiting the photocatalytic process [45].

In order to discriminate the active radicals during degradation and further propose a photocatalysis mechanism, active radicals trapping experiments were carried out over the sample 5%AgWTS by means of the introduction of suitable scavenger such as IPA and EDTA-2Na for hydroxyl radicals •OH and holes, respectively. Remarkably, the addition of EDTA-2Na has no effect on the degrada-

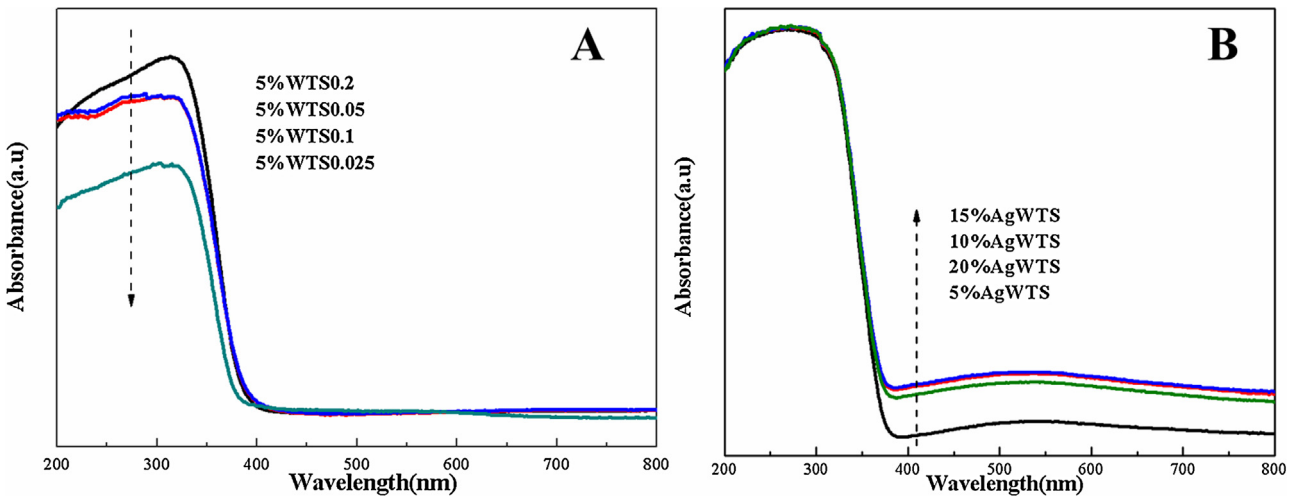

Fig. 4. (A) UV–vis diffuse reflectance spectra of 5%WTSx series (A) and xAgWTS series (B).

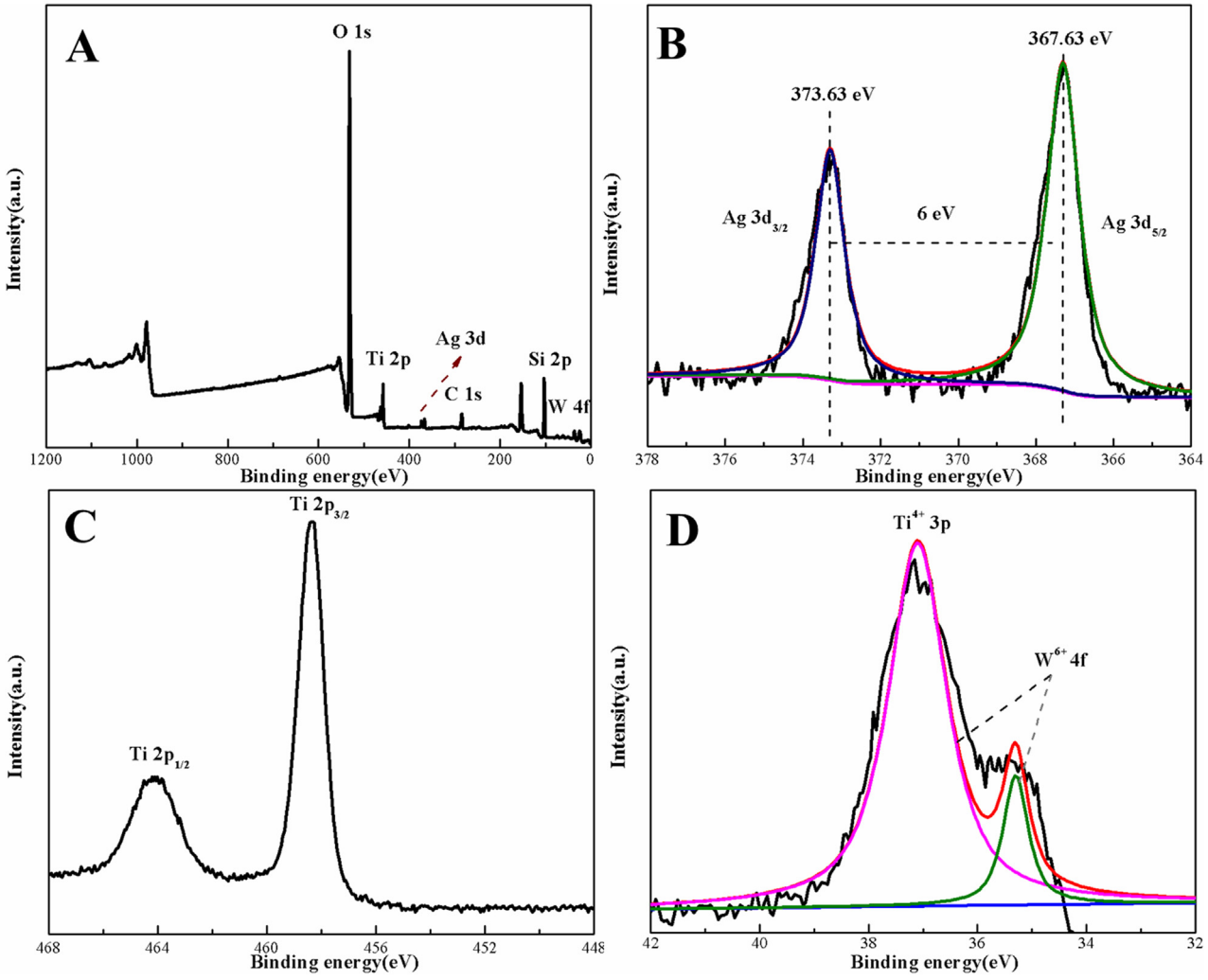

Fig. 5. XPS analysis of the sample 5%AgWTS: (A) survey spectra, (B) Ag 3d, (C) Ti 2p, (D) W 4f.

tion efficiency in Fig. 7A. However, the photocatalytic performance is greatly retarded as soon as IPA was added, indicating radicals •OH instead of holes exert dominant role in catalytic decomposition. In addition, the remarkable decrease of NBT concentration is indicative of the generation of superoxide radicals $\cdot O_2^-$. On the basis of above results, radicals $^{\bullet}O_2^-$ and •OH are predominate species that greatly promote the photocatalytic efficiency. The standard deviation bar of each value was added in Figs. A2–A4.

According to active radicals entrapping experiments, a possible mechanism was eventually proposed as shown in Fig. 8. Under visible-light irradiation ($\lambda > 420$ nm), the component WO_3 tends to excite and promote electrons to transfer to the conduction band,

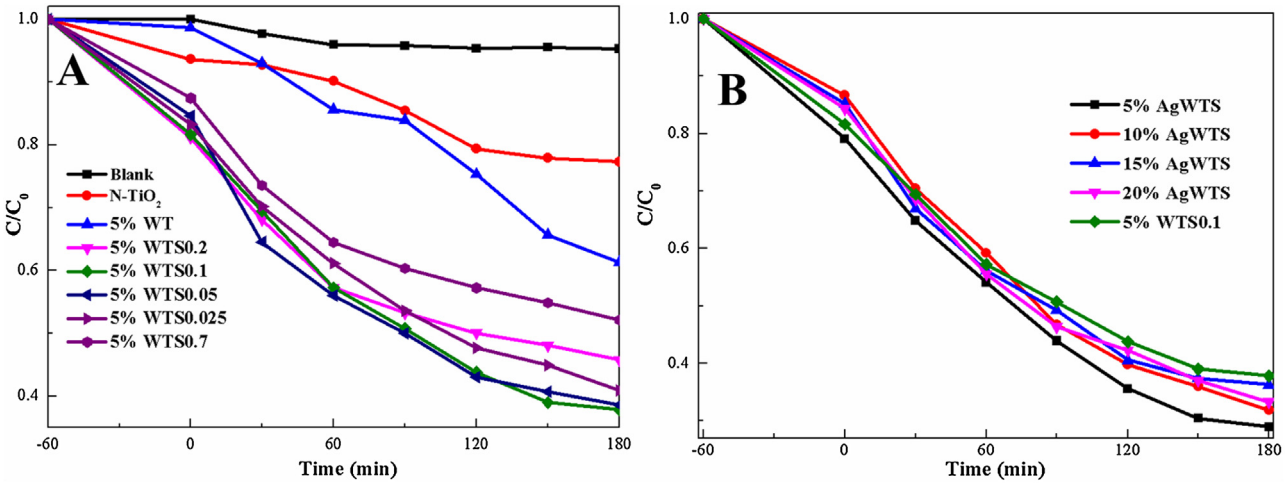

Fig. 6. Photocatalytic performances toward the degradation of RhB by 5%WTSx series, 5% WT and N-TiO_2 (A), and xAgWTS series (B).

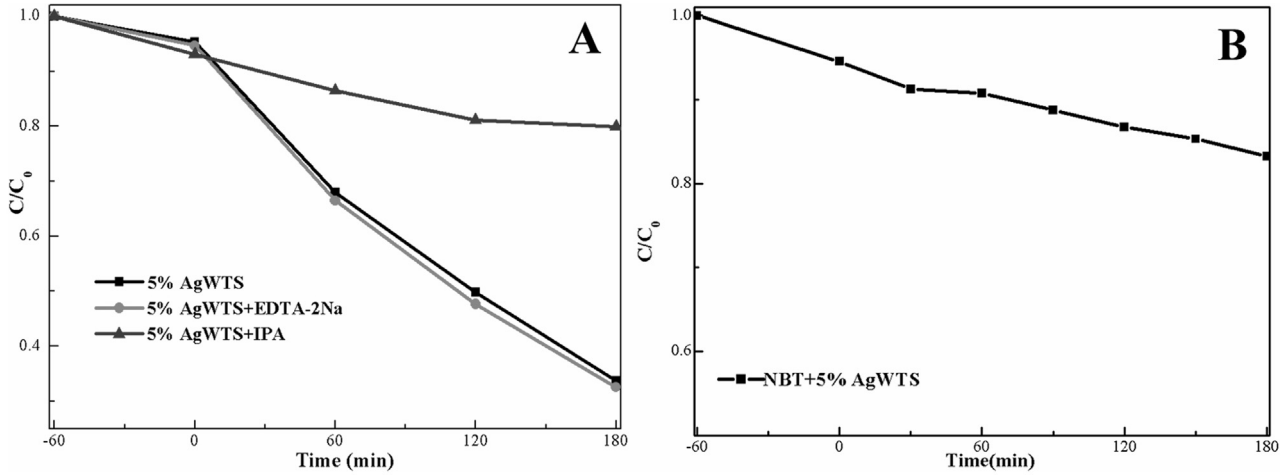

Fig. 7. Active species trapping experiments (A), and transformation percentage of NBT concentration (B) by using sample 5%AgWTS.

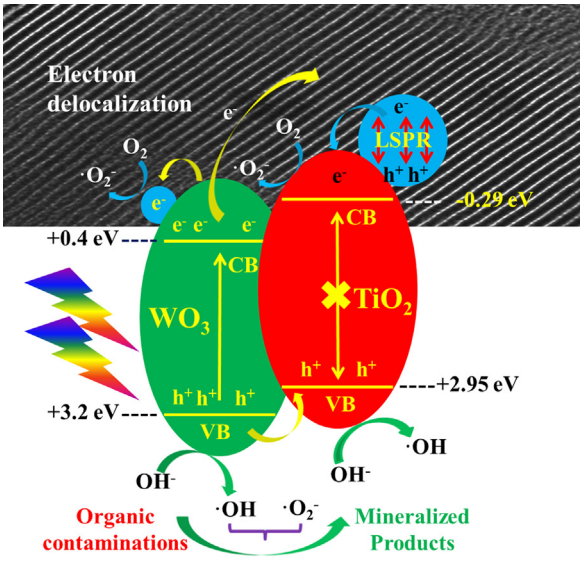

Fig. 8. Proposed mechanism of AgWTS composites upon visible light irradiation.

leaving holes on the valence band. TiO_2 is unable to excite because of the wide band gap. The photogenerated electrons on WO_3 conduction band are insufficient to reduce dissolved oxygen to produce radicals $^{\bullet}O_2^-$, instead, they can migrate and transfer to metallic Ag sites via the Schottky barrier at interface between metal and semiconductor phase. In addition, the holes collected on WO_3 valence band can thermodynamically transfer to valance band of TiO_2 and further oxidatively convert OH^- or water to radicals $^{\bullet}OH$ since the potential of valence band maximum E_{VBM} (+2.95 eV) is more positive than $E(^{\bullet}OH/OH^-)$ (+1.99 eV) and $E(^{\bullet}OH/H_2O)$ (+2.68 eV) [46,47]. In addition, metallic Ag tends to excite under visible light irradiation as a result of LSPR effect and the produced hot electrons can inject to the conduction band of TiO_2 and thus react with dissolved oxygen to form radicals $^{\bullet}O_2^-$ since the potential of conduction band minimum E_{CBM} (−0.29 eV) is much negative than $E(^{\bullet}O_2^-/O_2)$ (−0.046 eV) [47]. The formation of radicals $^{\bullet}O_2^-$ that was unavailable in WTS composites [32] can be successfully achieved in metallic Ag-contained WTS analogs, mainly attributing to the presence of LSPR generated hot electrons that are of high reductive capability. In addition, the retained electrons on the WO_3 valence band can disperse onto the SBA-15 matrix by means of electron delocalization effect [20], thus promoting the photocatalytic performance through the efficient inhibition of recombination process.

4. Conclusion

In this study, a series of mesoporous W-Ti-SBA15 composites and their Ag-deposited analogs were constructed and fully characterized by various techniques. It was found that original mesoporous structures were well remained and semiconductor clusters in SBA-15 matrix were gradually decreased in size along with the debatement of TiO_2/SiO_2 mass ratio. The deposition of Ag had almost no effect on the morphology, microstructure, and textural properties of composites. However, the visible-light absorption capability of composites was significantly enhanced due to the LSPR effect induced by the metallic Ag deposited. As for the degradation of dye RhB under visible light irradiation, as-synthesized WTS composites showed satisfactory photocatalytic efficiency that could be further enhanced by using Ag-contained ternary plasmonic composites. The enhancement of photocatalytic performance was discussed and a possible photocatalysis mechanism was finally proposed basing upon reactive radical species trapping experiments.

Acknowledgements

The research was financially supported by the National Natural Science Foundation of China (No. 21207089), the project-sponsored by SRF for ROCS, SEM., the Hujiang Foundation of China (No. B14003), the Innovation Program of Shanghai Municipal Education Commission (No. 14ZZ136), and the Natural Science Foundation of Shanghai (No. 13ZR1427600).

Appendix A.

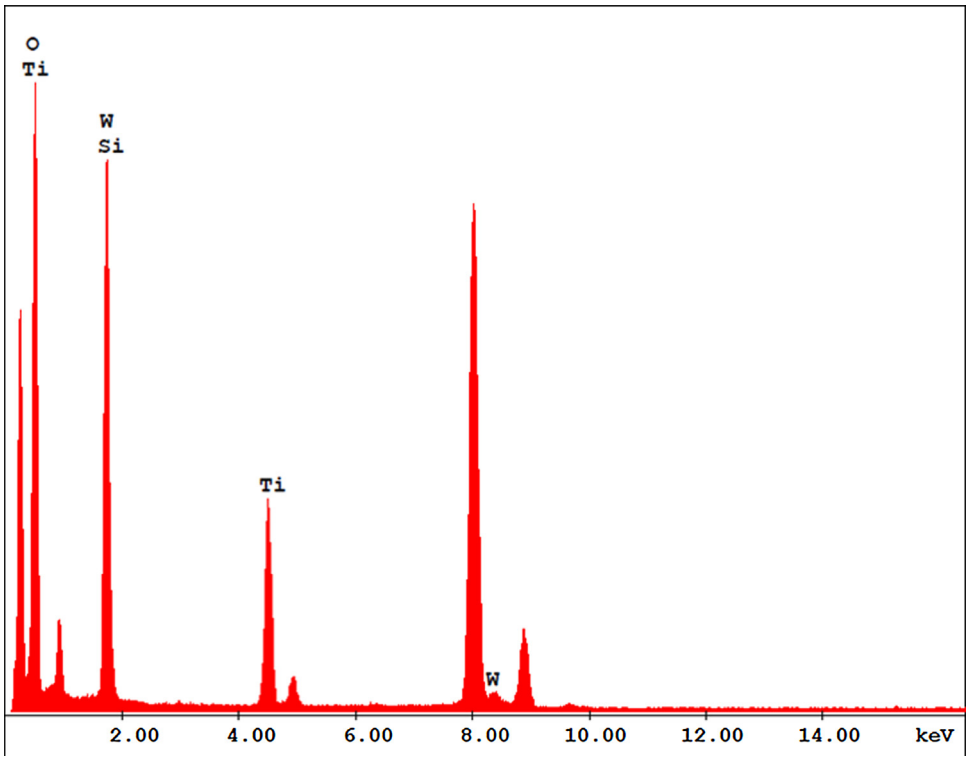

Fig. A1. EDS analysis of the sample 5%WTS0.1.

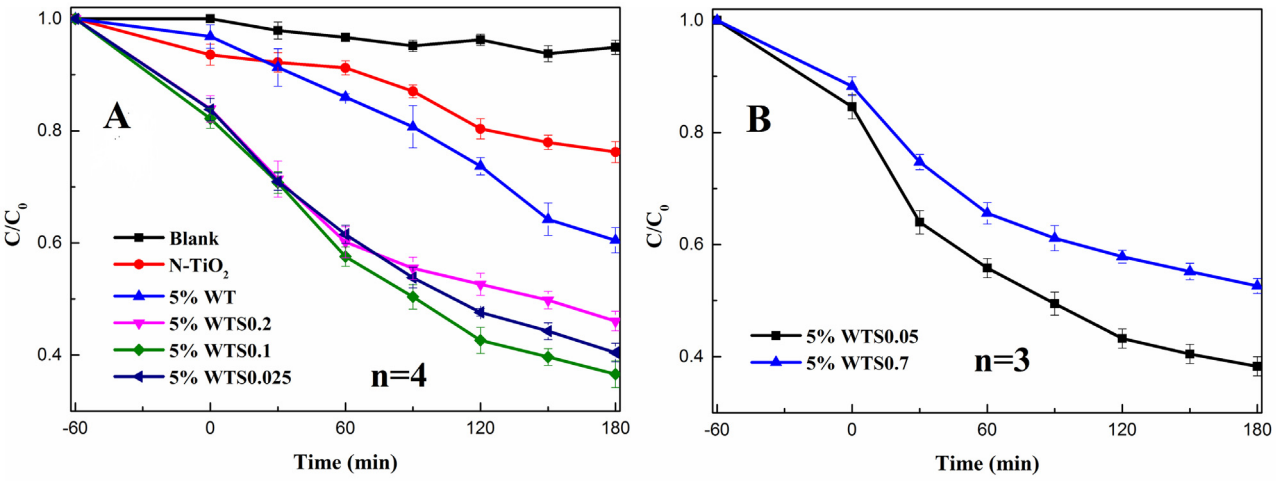

Fig. A2. Photocatalytic performances toward the degradation of RhB with standard deviation bars by 5%WTSx series, 5% WT and N-TiO_2 (A and B).

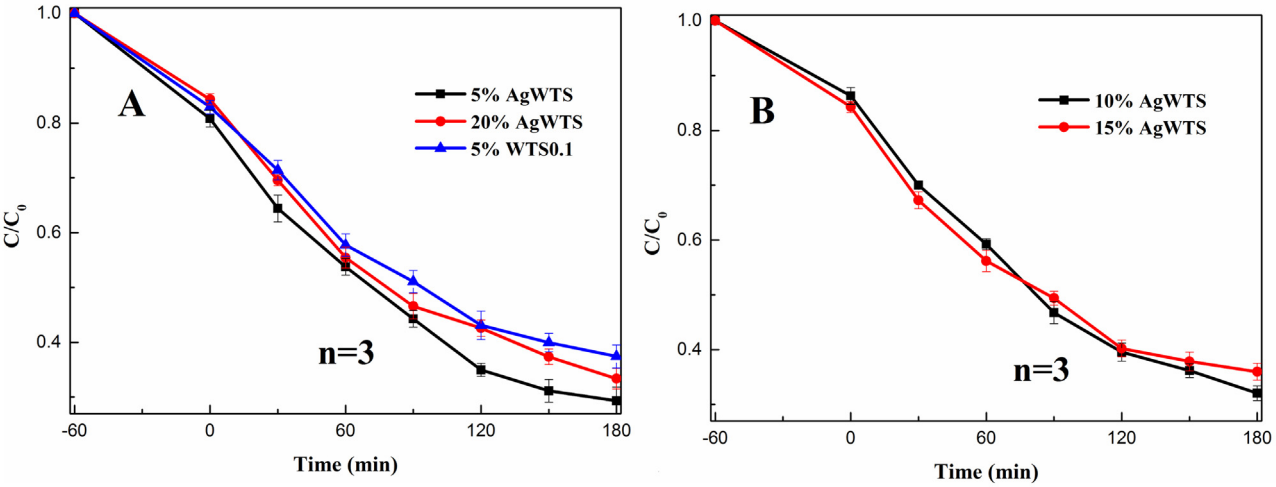

Fig. A3. Photocatalytic performances toward the degradation of RhB with standard deviation bars by xAgWTS series (A and B).

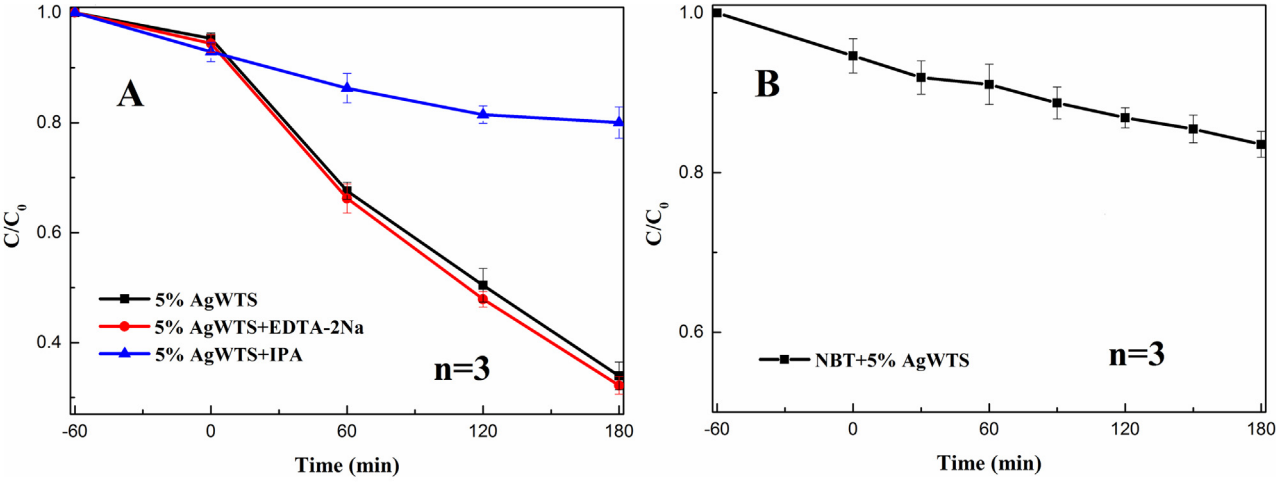

Fig. A4. Active species trapping experiments (A), and transformation percentage of NBT concentration (B) by using sample 5%AgWTS with standard deviation bars.

References

[1] M. Kapilashrami, Y.F. Zhang, Y.S. Liu, A. Hagfeldt, J.H. Guo, Probing the optical property and electronic structure of TiO_2 nanomaterials for renewable energy applications, Chem. Rev. 114 (2014) 9662–9707.

[2] Y. Ma, X.L. Wang, Y.S. Jia, X.B. Chen, H.X. Han, C. Li, Titanium dioxide-based nanomaterials for photocatalytic fuel generations, Chem. Rev. 114 (2014) 9987–10043.

[3] T.L. Thompson, J.T. Yates, Surface science studies of the photoactivation of TiO_2-new photochemical processes, Chem. Rev. 106 (2006) 4428–4453.

[4] Y.J. Wang, Q.S. Wang, X.Y. Zhan, F.M. Wang, M. Safdar, J. He, Visible light driven type II heterostructures and their enhanced photocatalysis properties: a review, Nanoscale 5 (2013) 8326–8339.

[5] H. Dong, G. Zeng, L. Tang, C. Fan, C. Zhang, X. He, Y. He, An overview on limitations of TiO_2-based particles for photocatalytic degradation of organic pollutants and the corresponding countermeasures, Water Res. 79 (2015) 128–146.

[6] M.S. Bazarjani, M. Hojamberdiev, K. Morita, G. Zhu, G. Cherkashinin, C. Fasel, T. Herrmann, H. Breitzke, A. Gurlo, R. Riedel, Visible light photocatalysis with c-$WO_{3-x}/WO_{(3)x}H_{(2)O}$ nanoheterostructures in situ formed in mesoporous polycarbosilane-siloxane polymer, J. Am. Chem. Soc. 135 (2013) 4467–4475.

[7] A. Hiskia, A. Mylonas, E. Papaconstantinou, Comparison of the photoredox properties of polyoxometallates and semiconducting particles, Chem. Soc. Rev. 30 (2001) 62–69.

[8] A. Alonso-Tellez, D. Robert, V. Keller, N. Keller, H_2S photocatalytic oxidation over WO_3/TiO_2 Hombikat UV100, Environ. Sci. Pollut. Res. 21 (2014) 3503–3514.

[9] O. Lorret, D. Francova, G. Waldner, N. Stelzer, W-doped titania nanoparticles for UV and visible-light photocatalytic reactions, Appl. Catal. B 91 (2009) 39–46.

[10] K. Lv, J. Li, X. Qing, W. Li, Q. Chen, Synthesis and photo-degradation application of WO_3/TiO_2 hollow spheres, J. Hazard. Mater. 189 (2011) 329–335.

[11] V. Puddu, R. Mokaya, G.L. Puma, Novel one step hydrothermal synthesis of WO_3/TiO_2 nanocomposites with enhanced photocatalytic activity, Chem. Commun. (2007) 4749–4751.

[12] D. Su, J. Wang, Y. Tang, C. Liu, L. Liu, X. Han, Constructing WO_3/TiO_2 composite structure towards sufficient use of solar energy, Chem. Commun. 47 (2011) 4231–4233.

[13] K.K. Akurati, A. Vital, J.-P. Dellemann, K. Michalow, T. Graule, D. Fetti, A. Baiker, Flame-made WO_3/TiO_2 nanoparticles: relation between surface acidity, structure and photocatalytic activity, Appl. Catal. B 79 (2008) 53–62.

[14] Y. Liu, C.S. Xie, H.Y. Li, H. Chen, T. Zou, D.W. Zeng, Improvement of gaseous pollutant photocatalysis with WO_3/TiO_2 heterojunctional-electrical layered system, J. Hazard. Mater. 196 (2011) 52–58.

[15] A.O.T. Patrocinio, L.F. Paula, R.M. Paniago, J. Freitag, D.W. Bahnemann, Layer-by-layer WO_3/TiO_2 thin films as efficient photocatalytic self-cleaning surfaces, ACS Appl. Mater. Interfaces 6 (2014) 16859–16866.

[16] A.K.L. Sajjad, S. Shamaila, B. Tian, F. Chen, J. Zhang, Comparative studies of operational parameters of degradation of azo dyes in visible light by highly efficient WO_x/TiO_2 photocatalyst, J. Hazard. Mater. 177 (2010) 781–791.

[17] A.K.L. Sajjad, S. Shamaila, B.Z. Tian, F. Chen, J.L. Zhang, One step activation of WO_x/TiO_2 nanocomposites with enhanced photocatalytic activity, Appl. Catal. B 91 (2009) 397–405.

[18] Y. Yuan, Y. Zhao, H. Li, Y. Li, X. Gao, C. Zheng, J. Zhang, Electrospun metal oxide-TiO_2 nanofibers for elemental mercury removal from flue gas, J. Hazard. Mater. 227 (2012) 427–435.

[19] S. Perathoner, P. Lanzafame, R. Passalacqua, G. Centi, R. Schlogl, D.S. Su, Use of mesoporous SBA-15 for nanostructuring titania for photocatalytic applications, Microporous Mesoporous Mater. 90 (2006) 347–361.

[20] M.V.P. Sharma, V.D. Kumari, M. Subrahmanyam, TiO(2) supported over SBA-15: an efficient photocatalyst for the pesticide degradation using solar light, Chemosphere 73 (2008) 1562–1569.
[21] W. Wang, M. Song, Photocatalytic activity of titania-containing mesoporous SBA-15 silica, Microporous Mesoporous Mater. 96 (2006) 255–261.
[22] D.Y. Zhao, J.L. Feng, Q.S. Huo, N. Melosh, G.H. Fredrickson, B.F. Chmelka, G.D. Stucky, Triblock copolymer syntheses of mesoporous silica with periodic 50 to 300 angstrom pores, Science 279 (1998) 548–552.
[23] G.P. Li, Y.X. Wang, L.Q. Mao, Recent progress in highly efficient Ag-based visible-light photocatalysts, RSC Adv. 4 (2014) 53649–53661.
[24] Z.Z. Lou, Z.Y. Wang, B.B. Huang, Y. Dai, Synthesis and activity of plasmonic photocatalysts, ChemCatChem 6 (2014) 2456–2476.
[25] S. Sarina, E.R. Waclawik, H.Y. Zhu, Photocatalysis on supported gold and silver nanoparticles under ultraviolet and visible light irradiation, Green Chem. 15 (2013) 1814–1833.
[26] J.B. Fei, J.B. Li, Controlled preparation of porous TiO_2–Ag nanostructures through supramolecular assembly for plasmon-enhanced photocatalysis, Adv. Mater. 27 (2015) 314–319.
[27] J.B. Fei, Y. Cui, J. Zhao, L. Gao, Y. Yang, J.B. Li, Large-scale preparation of 3D self-assembled iron hydroxide and oxide hierarchical nanostructures and their applications for water treatment, J. Mater. Chem. 21 (2011) 11742–11746.
[28] J.B. Fei, L. Gao, J. Zhao, C.L. Du, J.B. Li, Responsive helical self-assembly of $AgNO_3$ and melamine through asymmetric coordination for Ag nanochain synthesis, Small 9 (2013) 1021–1024.
[29] F. Chang, J. Wang, J.R. Luo, J.R. Sun, B.Q. Deng, X.F. Hu, Enhanced visible-light-driven photocatalytic performance of mesoporous W-Ti-SBA-15 prepared through a facile hydrothermal route, Colloids Surf. A 499 (2016) 69–78.
[30] T.T. Li, L.H. Zhao, Y.M. He, J. Cai, M.F. Luo, J.J. Lin, Synthesis of g-C_3N_4/$SmVO_4$ composite photocatalyst with improved visible light photocatalytic activities in RhB degradation, Appl. Catal. B 129 (2013) 255–263.
[31] F. Chang, J. Zhang, Y.C. Xie, J. Chen, C.L. Li, J. Wang, J.R. Luo, B.Q. Deng, X.F. Hu, Fabrication, characterization, and photocatalytic performance of exfoliated g-C_3N_4-TiO_2 hybrids, Appl. Surf. Sci. 311 (2014) 574–581.
[32] X.F. Hu, T. Mohamood, W.H. Ma, C.C. Chen, J.C. Zhao, Oxidative decomposition of rhodamine B dye in the presence of VO^{2+} and/or Pt(IV) under visible light irradiation: N-deethylation, chromophore cleavage, and mineralization, J. Phys. Chem. B 110 (2006) 26012–26018.
[33] L.Q. Ye, J.Y. Liu, Z. Jiang, T.Y. Peng, L. Zan, Facets coupling of BiOBr- g-C_3N_4 composite photocatalyst for enhanced visible-light-driven photocatalytic activity, Appl. Catal. B 142 (2013) 1–7.
[34] J.E. Herrera, J.H. Kwak, J.Z. Hu, Y. Wang, C.H.F. Peden, J. Macht, E. Iglesia, Synthesis, characterization, and catalytic function of novel highly dispersed tungsten oxide catalysts on inesoporous silica, J. Catal. 239 (2006) 200–211.
[35] X. Zhang, F. Zhang, K.Y. Chan, Synthesis of titania-silica mixed oxide mesoporous materials, characterization and photocatalytic properties, Appl. Catal. A 284 (2005) 193–198.
[36] L. Zhao, J.G. Yu, Controlled synthesis of highly dispersed TiO_2 nanoparticles using SBA-15 as hard template, J. Colloid Interface Sci. 304 (2006) 84–91.
[37] X.Z. Li, F.B. Li, C.L. Yang, W.K. Ge, Photocatalytic activity of WO_x-TiO_2 under visible light irradiation, J. Photochem. Photobiol. A 141 (2001) 209–217.
[38] X.H. Zhang, L.L. Wang, C.B. Liu, Y.B. Ding, S.Q. Zhang, Y.X. Zeng, Y.T. Liu, S.L. Luo, A bamboo-inspired hierarchical nanoarchitecture of Ag/CuO/TiO_2 nanotube array for highly photocatalytic degradation of 2,4-dinitrophenol, J. Hazard. Mater. 313 (2016) 244–252.
[39] J.-C. Hu, Y.-D. Wang, L.-F. Chen, R. Richards, W.-M. Yang, Z.-C. Liu, W. Xu, Synthesis and characterization of tungsten-substituted SBA-15: an enhanced catalyst for 1-butene metathesis, Microporous Mesoporous Mater. 93 (2006) 158–163.
[40] K. De Witte, A.M. Busuioc, V. Meynen, M. Mertens, N. Bilba, G. Van Tendeloo, P. Cool, E.F. Vansant, Influence of the synthesis parameters of TiO_2-SBA-15 materials on the adsorption and photodegradation of rhodamine-6G, Microporous Mesoporous Mater. 110 (2008) 100–110.
[41] W.Y. Jung, S.H. Baek, J.S. Yang, K.T. Lim, M.S. Lee, G.D. Lee, S.S. Park, S.S. Hong, Synthesis of Ti-containing SBA-15 materials and studies on their photocatalytic decomposition of orange II, Catal. Today 131 (2008) 437–443.
[42] A. Sarkar, S. Kapoor, T. Mukherjee, Synthesis and characterisation of silver nanoparticles in viscous solvents and its transfer into non-polar solvents, Res. Chem. Intermed. 36 (2010) 411–421.
[43] Y.N. Zhang, H.Q. Fan, M.M. Li, H.L. Tian, Ag/$BiPO_4$ heterostructures: synthesis, characterization and their enhanced photocatalytic properties, Dalton Trans. 42 (2013) 13172–13178.
[44] Y. Cao, J. Wang, M. Kang, Y. Zhu, Efficient synthesis of ethylene glycol from cellulose over Ni-WO_3/SBA-15 catalysts, J. Mol. Catal. A 381 (2014) 46–53.
[45] H. Liu, W.R. Cao, Y. Su, Y. Wang, X.H. Wang, Synthesis, characterization and photocatalytic performance of novel visible-light-induced Ag/BiOI, Appl. Catal. B 111 (2012) 271–279.
[46] F. Dong, Z.W. Zhao, Y.J. Sun, Y.X. Zhang, S. Yan, Z.B. Wu, An advanced semimetal-organic Bi spheres-g-C_3N_4 nanohybrid with SPR-enhanced visible-light photocatalytic performance for no purification, Environ. Sci. Technol. 49 (2015) 12432–12440.
[47] H.F. Li, H.T. Yu, X. Quan, S. Chen, Y.B. Zhang, Uncovering the key role of the fermi level of the electron mediator in a Z-scheme photocatalyst by detecting the charge transfer process of WO_3-metal-g-C_3N_4 (metal = Cu, Ag Au), ACS Appl. Mater. Interfaces 8 (2016) 2111–2119.